The Journal of Chemical Physics ARTICLE scitation.org/journal/jcp

One-electron oxidation of TAT-motif triplex DNA and the ensuing Hoogsteen hydrogen-bonding dissociation

Cite as: J. Chem. Phys. 152, 035101 (2020); doi: 10.1063/1.5135769
Submitted: 8 November 2019 • Accepted: 26 December 2019 •
Published Online: 15 January 2020

Qian Zhou, Yinghui Wang, Xiaojuan Dai, Chunfan Yang, Jialong Jie, and Hongmei Su[a]

AFFILIATIONS

College of Chemistry, Beijing Normal University, Beijing 100875, People's Republic of China

[a]Author to whom correspondence should be addressed: hongmei@bnu.edu.cn

ABSTRACT

One-electron oxidation of adenine (A) leads initially to the formation of adenine radical cation ($A^{\bullet+}$). Subsequent deprotonation of $A^{\bullet+}$ can provoke deoxyribonucleic acid (DNA) damage, which further causes senescence, cancer formation, and even cell death. However, compared with considerable reports on $A^{\bullet+}$ reactions in free deoxyadenosine (dA) and duplex DNA, studies in non-B-form DNA that play critical biological roles are rare at present. It is thus of vital importance to explore non-B-form DNA, among which the triplex is an emerging topic. Herein, we investigate the deprotonation behavior of $A^{\bullet+}$ in the TAT triplex with continuous A bases by time-resolved laser flash photolysis. The rate constants for the one-oxidation of triplex 8.4×10^8 M^{-1} s^{-1} and $A^{\bullet+}$ deprotonation 1.3×10^7 s^{-1} are obtained. The kinetic isotope effect of $A^{\bullet+}$ deprotonation in the TAT triplex is 1.8, which is characteristic of a direct release of the proton into the solvent similar to free base dA. It is thus elucidated that the $A^{\bullet+}$ proton bound with the third strand is most likely to be released into the solvent because of the weaker Hoogsteen H-bonding interaction and the presence of the highly mobile hydration waters within the third strand. Additionally, it is confirmed through Fourier transform infrared spectroscopy that the deprotonation of $A^{\bullet+}$ results in the dissociation of the third strand and disruption of the secondary structure of the triplex. These results provide valuable kinetic data and in-depth mechanistic insights for understanding the adenine oxidative DNA damage in the triplex.

I. INTRODUCTION

Deoxyribonucleic acid (DNA) is the genetic material of an organism, and its oxidative damage can lead to faulty coding, causing senescence, cancer formation, and even cell death.[1,2] These types of damage can occur in various parts (nucleobase, deoxyribose, and phosphate) of the DNA, among which the base is the most vulnerable to oxidative damage.[3] One of the most common types of oxidative DNA damage is one-electron oxidation of nucleobases, which can occur during exposure of DNA to ionizing radiation or photosensitizers.[4,5] In the one-electron oxidation process, loss of an electron from DNA initially creates a radical cation, leading to a cascade of DNA damage reactions.[6,7] For adenine (A) upon one-electron oxidation (E^0 = 1.42 V),[8–11] the formed adenine radical cation ($A^{\bullet+}$) becomes acidic and has a pK_a of 4.0,[10–13] which drives the deprotonation to lose the N_6-H proton into bulk water generating adenine neutral radical [A(N6-H)$^{\bullet}$] with a rate constant of 2.0×10^7 s^{-1} in neutral solution [Scheme 1, Eq. (1)].[11,12,14] In duplex surroundings, N6-H_a in the A base is hydrogen bonded with O4 of the T base while the other proton N6-H_b is free [Scheme 1, Eq. (2)]. Thus, the free N6-H_b is considered to individually deprotonate into bulk water after one-electron oxidation of duplex DNA.[11,12] The deprotonation rate constants of $A^{\bullet+}$ in double-stranded oligonucleotides (ODNs) are 1.0–1.3 $\times 10^7$ s^{-1} for the duplex containing continuous A bases and 2.0×10^7 s^{-1} for the duplex containing alternating A•T bases.[11] In contrast, the deprotonation of N6-H_a that hydrogen bonded with O4 of the T base cannot occur because the pK_a values of $A^{\bullet+}$ (pKa = 4.0) and T(+H^+) (pK_a = −5) make this pathway infeasible.[9,12] Obviously, the proton surroundings have a significant effect on the $A^{\bullet+}$ deprotonation behavior.

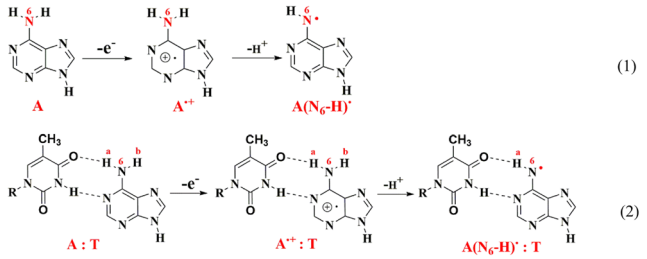

SCHEME 1. Reaction pathways of one-electron oxidation of A followed by deprotonation in free nucleotide (1) and in duplex A-T base pair (2).

Triplex is a family of triple helical DNA structures. Since Felsenfeld *et al.* first reported the formation of triplex DNA in 1957,[15] there has been growing evidence for the existence of triplex DNA in living organisms. It is formed when a single-stranded triplex-forming oligonucleotide (TFO) binds in the major groove of target duplex DNA by Hoogsteen (parallel triplex) or reverse Hoogsteen (antiparallel triplex) hydrogen bonding composed of C^+-G-C, G-G-C, A-A-T, or T-A-T base pair.[16–20] Due to the binding of the third strand to the major groove of the target duplex, the hydrogen bonding, solvent accessibility, and base stacking are changed significantly.[21–23] Our previous studies indicated that the deprotonation of $G^{\bullet+}$ in triplex DNA is different from that of free bases and duplex DNA, revealing structure-dependent degradation pathways and deprotonation behavior, where $G^{\bullet+}$ mainly suffers from fast deprotonation by release of both N1-H and N2-H of G in the third strand into bulk water.[6] This observation explains why strand breaks linked to $G^{\bullet+}$ deprotonation occur exclusively at G repeat sequences in the third strand of antiparallel DNA containing the GGC motif.[24]

For triplex DNA containing the TAT motif, where the third strand consists of continuous T bases and the target duplex is composed of continuous A and T bases, the deprotonation behavior of $A^{\bullet+}$ could also be affected by the unique TAT triplex structure. As shown in Scheme 2, the presence of the third strand widens the major groove and divides it into two asymmetric parts: the minor part of the major groove (MM-groove) and the major part of the major groove (MM-groove). The MM-groove of the TAT triplex is an interesting amphipathic structure, with an outer hydrophobic part formed by two methyl groups of the thymine bases and an inner hydrophilic part formed by the N6 and O4 polar groups of adenine and thymine. The amphipathic structure renders the waters in the MM-groove not in fixed positions but shows high mobility within the groove.[21] Such distinct structural features of the TAT triplex make it an interesting candidate to be examined. The formation of triplex structures may affect gene expression, dictate site-specific DNA damage, and have potential applications in photocrosslinking of duplex DNA, inhibition of protein-DNA binding, and in nanotechnology.[17,18,25–29] Thus, research on the underlying deprotonation molecular mechanism and dynamics of $A^{\bullet+}$ in triplex DNA is also of biological significance.

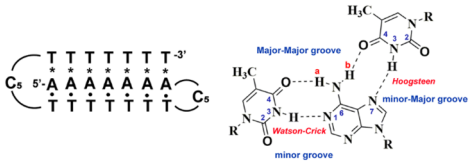

SCHEME 2. Schematic structure of the TAT triplex (TAT7) (in this notation, "*" and "•" represent Hoogsteen and Watson-Crick base pairing, respectively[30–35]).

In this context, we performed comprehensive time-resolved ultraviolet visible (UV-vis) absorption and Fourier transform infrared (FTIR) spectroscopy experiments to investigate the $A^{\bullet+}$ deprotonation process and the ensuing structural change induced by $A^{\bullet+}$ deprotonation in the TAT triplex $d(A_7C_5T_7C_5T_7)$ (denoted by TAT7), as shown in Scheme 2. Using the highly potent $SO_4^{\bullet-}$ radical to oxidize TAT7, the $A^{\bullet+}$ (hole) is produced and its subsequent deprotonation is directly detected by laser flash photolysis. The deprotonation rate 1.3×10^7 s^{-1} of $A^{\bullet+}$ within TAT7 is obtained, which is similar to that in the case of duplex containing continuous A bases.[11] By the further kinetic isotope effect experiment (KIE = 1.8), the deprotonation pathway of triplex DNA TAT7, which involves direct release of the proton of $A^{\bullet+}$ into the solvent, is elucidated.[36,37] Due to the weaker Hoogsteen H-bonding[26] as well as the presence of the highly mobile hydration waters in the MM-groove within the third strand,[21] the lost proton of $A^{\bullet+}$ should be the one bonded with the third strand. Furthermore, we noted that the infrared (IR) spectrum can successfully record the structural changes of the TAT7 triplex after one-electron oxidation, showing IR peaks characteristic of duplex structure, which is a striking indicator for the conversion from triplex to duplex as a consequence of $A^{\bullet+}$ deprotonation. These results demonstrate that the highly mobile hydration waters in the MM-groove of the TAT triplex play key roles in the $A^{\bullet+}$ deprotonation pathway and provide mechanistic insights to enrich the fundamental understanding of adenine oxidative damage of triplex DNA.

II. MATERIALS AND COMPUTATIONAL METHODS

A. Materials

2′-Deoxyadenine (dA, Alfa Aesar), sodium persulfate ($Na_2S_2O_8$, Sigma-Aldrich), and sodium phosphate buffer in H_2O and D_2O at pH 7.0 (10 mmol/l, Beijing Solarbio Science & Technology) were used as purchased. The DNA oligonucleotides TAT7(5′-AAAAAAACCCCCTTTTTTTCCCCCTTTTTTT-3′) and AT7(5′-AAAAAAACCCCCTTTTTTT-3′) were purchased from Sangon Biotech (Shanghai) Co., Ltd., in ULTRAPAGE-purified form. Single-strand concentrations were determined by monitoring the absorbance at 260 nm in the UV-vis spectra, and the corresponding extinction coefficients of 271 100 and 178 400M^{-1} cm^{-1} for TAT7 and AT7 were obtained from www.idtdna.com, respectively. The DNA oligonucleotides were prepared as follows: The samples were dissolved in 10 mM sodium phosphate buffer solution (H_2O) for TAT7 and 10 mM sodium phosphate buffer solution (D_2O) for TAT7 and AT7. The mixtures were heated to 90 °C for 20 min, then cooled down to room temperature at a cooling rate of 0.5 °C/min, and incubated at 4 °C for 12 h. The formation of triplex DNA and duplex DNA was confirmed by circular dichroism (CD) spectroscopy. All the reagents were used as received.

B. Circular dichroism spectroscopy

Circular dichroism experiments were performed at room temperature using a Jasco-815 spectropolarimeter. Each measurement was recorded from 200 to 400 nm in a 1 cm path length quartz cuvette at a scanning rate of 1000 nm/min. The final data were the average of three measurements. The concentration of DNA is 10 μM for TAT7 and AT7. The scan of the buffer alone was used as the background, which was subtracted from the average scan for each sample.

C. Laser flash photolysis

Nanosecond time-resolved absorption spectra were measured using a flash photolysis setup Edinburgh LP980 spectrometer (Edinburgh Instruments, Ltd.), combined with a Nd:YAG laser (Surelite II, Continuum, Inc.) as described previously. The sample was excited by a 355 nm laser pulse (1 Hz, 20 mJ/pulse, FWHM ≈7 ns). The analyzing light was from a 150 W pulsed xenon lamp. A monochromator equipped with a photomultiplier for collecting the spectral data in the range from 300 to 700 nm was used to analyze transient absorption spectra. Data were analyzed by the online software of the LP980 spectrophotometer, and the instrument response function of the Gaussian type was considered.

D. Generation of sulfate radical anions

Sulfate radical anions, $SO_4^{\bullet-}$, were generated by the photodissociation of peroxodisulfate anions ($S_2O_8^{2-}$) by nanosecond 355 nm laser pulses. Here, $Na_2S_2O_8$ is photolyzed as the $SO_4^{\bullet-}$ precursor,

$$S_2O_8^{2-} + h\nu \rightarrow 2SO_4^{\bullet-}.$$

The sulfate radical $SO_4^{\bullet-}$ has transient absorption with a resolved band at 450 nm and a shoulder at 330 nm, which is in good agreement with the spectra reported previously.[22,38] The photodissociation of $S_2O_8^{2-}$ is rapid, and all $SO_4^{\bullet-}$ are generated within the ~14 ns laser pulse duration. The concentration of $SO_4^{\bullet-}$ can be estimated by the absorbance at 450 nm using an extinction coefficient of 1600 M^{-1} cm^{-1},[39] giving a value of 30 μM, which is much smaller than the concentration of triplex DNA (at least 3.0 mM for TAT7). Additionally, it is expected that only the A base may be oxidized by $SO_4^{\bullet-}$, yielding an electron loss center in the triplex DNA initially.

E. Fourier transform infrared (FTIR) experiment

FTIR spectra of all DNA before and after laser irradiation were recorded using a Bruker Vertex 80 V. The TAT7 and AT7 were deposited between 2 mm thick CaF_2 windows at a 3 mM strand concentration. The solvent is 10 mM sodium phosphate buffer in D_2O at pH 7.0. The third harmonic of the Nd:YAG laser (355 nm) operating at a 1 Hz repetition rate was used in the experiments. The laser excitation beam was directed through an iris aperture (3 mm in diameter) and then overlapped with the infrared beam in the sample cell (100 μm optical path length) within the sample compartment of the FTIR spectrometer. The laser beam energy after the aperture was 20 mJ per pulse. The IR spectra were collected with a spectral resolution of 4 cm^{-1}.

F. Computational methods

The geometries of the TAT radical cation are optimized using B3LYP in connection with the 6-31++G (d, p) basis set in the polarized continuum model (PCM), which have been shown to be a sufficient and affordable computational method for studying DNA bases.[40–42] The calculation was carried out using the Gaussian 09 program package.[43]

III. RESULTS AND DISCUSSION

A. Characterizing the formation of triplex TAT7 and duplex AT7

The oligonucleotide sequence TAT7 (5′-$A_7C_5T_7C_5T_7$-3′) is chosen as the candidate for the investigation on the hydrogen-bonding effect of $A^{\bullet+}$ deprotonation. The oligonucleotide sequence TAT7 can fold back twice in pH 7.0 sodium phosphate buffer solution to form a TAT7 triplex with two pentamers (CCCCC) as the linker. The target duplex AT7 is formed by folding of the oligonucleotides sequence 5′-$A_7C_5T_7$-3′ composed of two heptamers linked with a CCCCC pentamer. The formation of the TAT7 triplex and the AT7 duplex is confirmed by circular dichroism spectra (CD spectra). As shown in Fig. 1, the TAT7 triplex DNA shows a characteristic CD signal consisting mainly of three positive peaks located at 280 nm, 262 nm (shoulder peak), and 222 nm as well as two negative peaks at 248 nm and 211 nm. The CD signal of AT7 duplex, which has characteristic positive peaks at 277 nm and 218 nm and a negative peak at 246 nm, reveals a significance difference from that of the TAT7 triplex. These results are in accord with previous studies, confirming the formation of the TAT7 triplex[26,33] and the AT7 duplex.[44]

B. Monitoring the one-electron oxidation of TAT7 triplex followed by $A^{\bullet+}$ deprotonation

The laser flash photolysis experiments below are all performed with a flowing quartz cuvette (1 × 1 cm), which ensures the fresh sample to be irradiated at each laser pulse. To assist in understanding the reaction in the TAT7 triplex, a reference experiment was first carried out for the one-electron oxidation of 2′-deoxyadenine (dA) by the $SO_4^{\bullet-}$ radical [Eq. (3)]. The $A^{\bullet+}$ in free dA is known to deprotonate N6-H forming A(N6-H)$^{\bullet}$ [Eq. (4)]. The transient

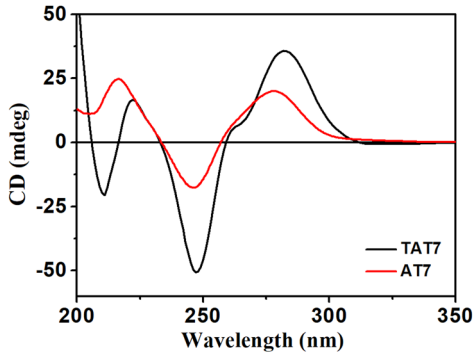

FIG. 1. CD spectra of TAT7 (black) and AT7 (red) in 10 mM sodium phosphate at pH 7.

absorption spectrum [Fig. 2(b)] shows one strong band at 330 nm and a flat absorption from 380 nm to 700 nm at 50 ns, which are in accordance with previous reports on the $A^{\bullet+}$ absorption character.[5,11] As the reaction time proceeds, the 330 nm band successively increases, accompanied by the formation of a broad absorption feature at ~ 600 nm and decay of the absorption band at 450 nm, as shown in the spectrum at 500 ns. This is the typical spectrum characteristic of $A^{\bullet+}$ deprotonation to form $A(N6\text{-}H)^{\bullet}$.[5,11] Given that $A(N6\text{-}H)^{\bullet}$ has larger absorption than $A^{\bullet+}$ at above 600 nm, the deprotonation rate constant is obtained by measuring the absorption change at 600 nm in 6.0 mM dA, at which concentration, the rate-determining step is the $A^{\bullet+}$ deprotonation according to the literature.[14] The measured deprotonation rate constant is $2.0 \times 10^7\ s^{-1}$ (within ~50 ns), which is the same as the previously reported value ($2.0 \times 10^7\ s^{-1}$).[11,14] This further confirms the assignment of the transient absorption features at 50 ns and 500 ns to $A^{\bullet+}$ and $A(N6\text{-}H)^{\bullet}$, respectively.

For the TAT7 triplex containing TAT motifs, all nucleobases are subject to oxidation by the instantaneously generated $SO_4^{\bullet-}$ upon 355 nm laser irradiation. Due to the lower oxidation potential of A than that of T and C, the initially formed electron loss centers should eventually be trapped by the A base to form the A radical cation. To confirm further where the oxidation will preferentially take place, the electronic configuration calculation of TAT was carried out at the level of PCM/B3LYP/6-31++G (d, p). It is noteworthy that almost all the highest occupied molecular orbital (HOMO) of TAT is concentrated on the A base [Fig. 2(a)]. This computational result confirms that the A base is initially oxidized.

Then, we performed laser flash photolysis experiments for the TAT7 triplex [Fig. 2(c)] upon one-electron oxidation by $SO_4^{\bullet-}$. Two peaks at 330 and 420 nm are observed at the early time (50 ns). These signals should originate from oxidation of the triplex TAT7 by $SO_4^{\bullet-}$ and its subsequent reactions. The 355 nm photolysis of the TAT7 triplex alone does not generate any signal. Different from the case in dA, it is noteworthy that in the spectra of TAT7, there are marked increases for the absorption intensities over the range of 400–500 nm and the absorption maximum shifts to 420 nm from 450 nm. These differences should arise from the π-stacking of consecutive A bases, since the cation radical $(AA)^{\bullet+}$ exists primarily in the stacked form as a dimer in the DNA strand, and the stacked dimer cation radicals are stabilized by the delocalization of the charge across two A bases.[11,45] Accompanying the decay of $(AA)^{\bullet+}$ at 420 nm, the absorbance at 330 nm increases and a broadband around 600 nm appears in the 500 ns spectrum, which is in line with the spectra of $A(N6\text{-}H)^{\bullet}$, indicating that $A^{\bullet+}$ in the TAT triplex deprotonates N6-H. The $A(N6\text{-}H)^{\bullet}$ spectral feature observed here in the triplex shows a weaker absorption intensity at 600 nm than that in the alternating adenine-thymine duplex.[46] This small difference might be related to the different base-pairing surrounding for the triplex and duplex. Furthermore, the decay kinetics of the 420 nm band and the formation kinetics of the 600 nm band in the TAT triplex are concomitant with each other (Fig. 3). Through monoexponential fitting, the decay lifetime of the 420 nm band is determined to be 80 ns and the growth lifetime of the 600 nm band is 76 ns. This means that the two absorbance changes should originate from the same reaction process, that is, the deprotonation of $A^{\bullet+}$ to $A(N6\text{-}H)^{\bullet}$. Moreover, it further confirms that the absorption band ~420 nm is the typical feature of $A^{\bullet+}$ in the DNA strand with consecutive stacked A bases, as of here, within the TAT triplex,

$$SO_4^{\bullet-} + A \rightarrow SO_4^{2-} + A^{\bullet+}, \quad (3)$$

$$A^{\bullet+} \rightarrow A(N_6\text{–}H)^{\bullet} + H^{+}. \quad (4)$$

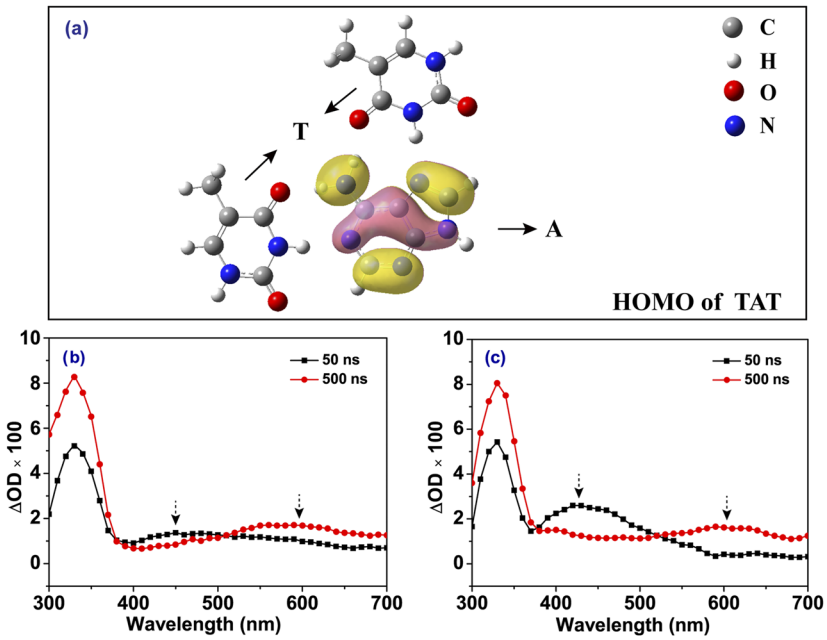

FIG. 2. (a) Orbital contour plot of the HOMO of TAT obtained by density functional calculation using GAUSSIAN 09 at the B3LYP/6-31++G (d, p) level. (b) Transient UV-vis spectra monitored at 50 ns (black squares) and 500 ns (red circles) for sodium phosphate buffer solution (pH = 7.0) of dA (6 mM) + $Na_2S_2O_8$ (600 mM) upon 355 nm laser excitation. (c) Transient UV-vis spectra monitored at 50 ns (black squares) and 500 ns (red circles) for sodium phosphate buffer solution (pH = 7.0) of TAT ([TAT7] = 3 mM) +$Na_2S_2O_8$ (600 mM) upon 355 nm laser excitation.

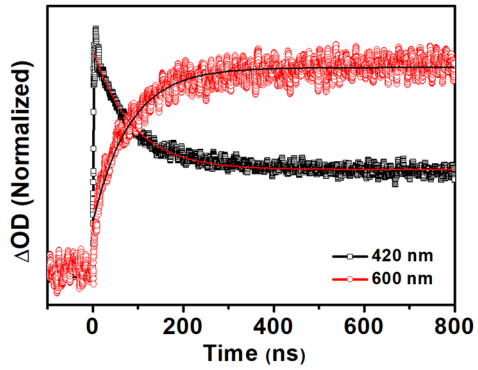

FIG. 3. Kinetics traces of TAT7 for $A^{\bullet+}$ decay at 420 nm (black) with the single-exponential fits to the data (solid red line) and $A(N_6\text{-}H)^{\bullet}$ growth at 600 nm (red) with the single-exponential fits to the data (solid black line).

The deprotonation rate constant is obtained by monitoring the growth kinetics of the 600 nm band. The concentration dependence of the 600 nm formation kinetics is assessed by varying the TAT7 triplex concentration from 1.0 mM to 4.0 mM (as the reaction site within TAT7 is actually A bases, the concentration of the A base is seven times greater than that of TAT7), as shown in Fig. 4(a). By fitting the kinetic curve at 600 nm, the reaction rate at different concentrations can be obtained. As shown in Fig. 4(b), the plot of the rate constant vs the concentration of the TAT7 triplex exhibits a linear relationship below 3 mM, indicating that the rate-determining step is the bimolecular reaction of A oxidation in TAT7 by $SO_4^{\bullet-}$. From the slope, the second-order oxidation rate constant is determined to be 8.4×10^8 M^{-1} s^{-1}. It shows here that the oxidation rate constant of the TAT7 triplex by $SO_4^{\bullet-}$ is smaller than that of the free base dA ($4.0 \times 10^9 M^{-1}$ s^{-1}).[14] Then, the rate constant reaches a plateau above 3.0 mM and is independent of the TAT concentration, which is ascribed to the first-order deprotonation process of $A^{\bullet+}$. The $A^{\bullet+}$ deprotonation rate constant in the TAT7 triplex is thus determined to be 1.3×10^7 s^{-1}, which is similar to that in duplex containing continuous A bases ($1.0–1.3 \times 10^7$ s^{-1}).[11]

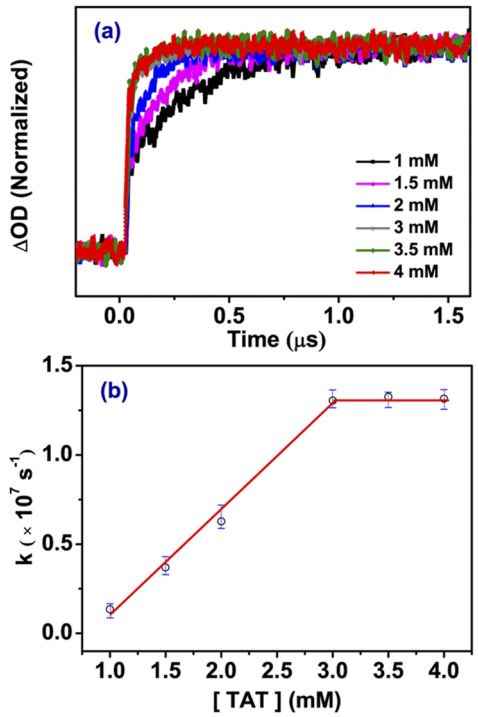

FIG. 4. (a) Kinetics traces for $A(N_6\text{-}H)^{\bullet}$ growth at 600 nm at different triplex concentrations. (b) Concentration dependence of $A(N_6\text{-}H)^{\bullet}$ formation rate constant obtained from the absorbance changes at 600 nm.

C. Elucidating the $A^{\bullet+}$ deprotonation mechanisms

It is known that the proton surroundings would have a significant influence on the deprotonation site. In free dA, $A^{\bullet+}$ mainly loses the N_6-H proton directly into bulk water, generating a neutral adenine radical [A(N6-H)•] [Scheme 1, Eq. (1)]. However, when $A^{\bullet+}$ locates in the AT base pair, the free proton N6-H of A is deprotonated [Scheme 1, Eq. (2)], whereas the proton transfer from N6-H of A to O4 of T through the hydrogen bonding is thermodynamically unfavorable.[9,12] For the TAT7 triplex, two active amino protons (N6-H) of the A base are both hydrogen bonded with O4 of two T bases, respectively. After one-electron oxidation of the TAT triplex to form $A^{\bullet+}$, which proton is released?

In fact, the surroundings of these two amino protons are different. As shown in Scheme 2, one N6—H participates in a base pair by Watson-Crick hydrogen bonding with O4 of the T base, but another one participates in a base pair with the T base located in the third strand by Hoogsteen hydrogen bonding. It has been verified that the dissociation of the third strand occurs at 34 °C, while disruption of the Watson-Crick duplex is observed at 60 °C.[26,31] This suggests that Hoogsteen hydrogen bonding that links the third strand to the target duplex is weaker than the Watson-Crick hydrogen bonding within the target duplex, and thus, the Hoogsteen-bound N6-H of A is easier to undergo deprotonation. Furthermore, the binding of the third strand in the major groove of the target duplex alters the solvent accessibility significantly, and the inner hydrophilic part formed by the N6 and O4 polar groups of adenine and thymine contains waters that show high mobility within the groove.[21] This structural feature causes the amino protons of the A base that form hydrogen bond with the T base of the third strand to come into contact with the solvent water molecule, incurring a character similar to that of the free A base. These analyses of the structural characteristic of the TAT triplex indicate that the N6-H proton involved in Hoogsteen hydrogen bonding with T in the third strand is nearly free and the other one in the target duplex is tightly bounded.

According to previous results, the kinetic isotope effect (KIE) on the deprotonation rate for free protons and tightly bound (hydrogen bonded) protons should be different. The KIE of $G^{\bullet+}$ deprotonation for free proton was reported to be 1.7, whereas the KIE for the tightly bound proton was 3.8.[36,37] Hence, we perform KIE experiments to examine the deprotonation site of $A^{\bullet+}$ in the TAT triplex. We first measured the $A^{\bullet+}$ deprotonation rate constant in free base dA as a standard reference. Figure 5(a) compares the absorbance

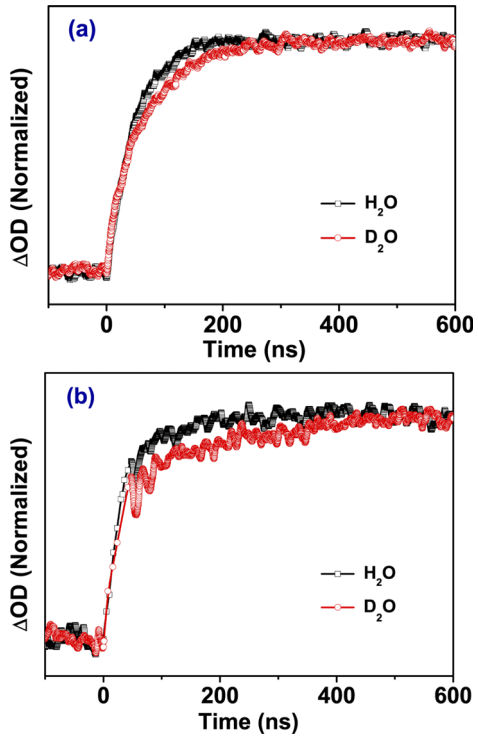

FIG. 5. (a) Absorbance changes at 600 nm after 355 nm laser flash photolysis of dA (6 mM) and $Na_2S_2O_8$ (600 mM) in 10 mM sodium phosphate buffer in H_2O at pH 7.0 (black) or in D_2O at pD 7.0 (red). (b) Absorbance changes at 600 nm after 355 nm laser flash photolysis of TAT (3 mM) and $Na_2S_2O_8$ (600 mM) in 10 mM sodium phosphate buffer in H_2O at pH 7.0 (black) or in D_2O at pD 7.0 (red).

changes at 600 nm after one-electron oxidation of free base dA by $SO_4^{\bullet-}$ in H_2O and D_2O. The deprotonation rate constants obtained from Fig. 5(a) are $k_{H_2O} = 2.1 \times 10^7\ s^{-1}$ and $k_{D_2O} = 1.3 \times 10^7\ s^{-1}$ from which the KIE of 1.6 is obtained.

Similar KIE experiments were performed for the TAT7 triplex. As seen in Fig. 5(b), the deprotonation rate in D_2O is markedly slower than that in H_2O, revealing obvious KIE. The deprotonation rate constants of $A^{\bullet+}$ are $k_{H_2O} = 1.3 \times 10^7\ s^{-1}$ and $k_{D_2O} = 7.2 \times 10^6\ s^{-1}$, from which the KIE of 1.8 is obtained for the TAT7 triplex. This value is about the same as that for free proton in dA, indicating that for $A^{\bullet+}$ in the TAT7 triplex, the proton involved in the H-bonding with T in the third strand (labeled N6-H_b in Scheme 2) is released directly into the solvent.

D. Monitoring the structural change of the TAT triplex after one-electron oxidation

Due to the weak interaction between the third strand and the homopurine strand of the target duplex as well as the existence of highly mobile hydration waters, it seems that the loss of Hoogsteen hydrogen bonded protons in triplex DNA is favorable. Upon loss of N6-H of A in the TAT triplex, the Hoogsteen hydrogen bonding could be destroyed. An interesting question arises regarding the consequence on the structure of TAT triplex DNA after deprotonation of the N6-H of $A^{\bullet+}$ in the third strand into the solvent. Will it cause the third strand dissociation and the destruction of the TAT triplex structure? Here, CD spectroscopy is not applicable to measure the change in the DNA structure after one-electron oxidation because the coexistent sodium persulfate $Na_2S_2O_8$ in the system absorbs strongly at 200–400 nm causing voltage oversaturation and obscure of the CD signal related to DNA structure. The steady-state FTIR measurements are thus performed to monitor the ensuing change after $A^{\bullet+}$ deprotonation by taking advantage of the characteristic IR bands in discerning the in-plane double-bond stretching vibrations (1600–1800 cm^{-1}). Indeed, the IR spectroscopy is a powerful technique to study the structures of triplex and duplex.[31] It is known that these IR bands are particularly sensitive to base-pairing interactions in this region.

The FTIR experiments are first performed for the TAT7 triplex and its target duplex AT7. For the triplex, the IR spectrum contains three obvious absorption bands located at 1696 cm^{-1},

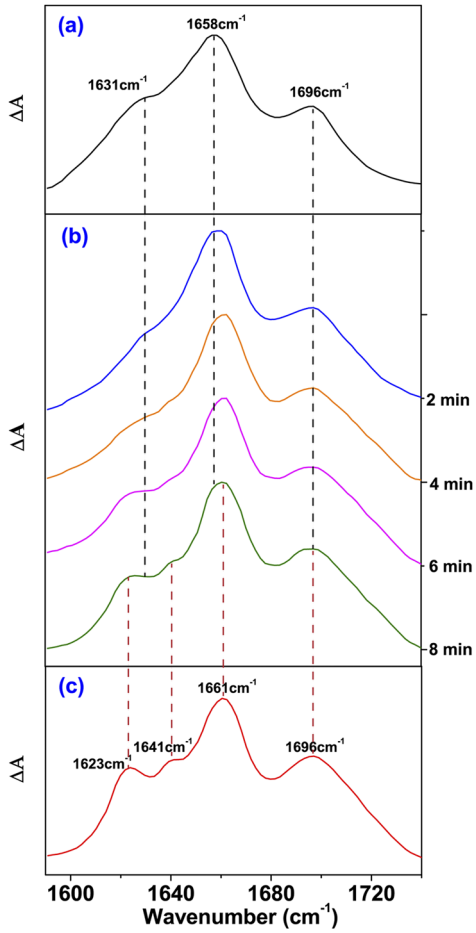

FIG. 6. (a) Steady-state FTIR spectra for triplex DNA ([TAT7] = 3 mM) + $Na_2S_2O_8$ (600 mM) at pD 7.0 (black); (b) steady-state FTIR spectra for triplex DNA ([TAT7] = 3 mM) + $Na_2S_2O_8$ (600 mM) at pD 7.0 after 2 min (blue), 4 min (orange), 6 min (pink), and 8 min (green) of 355 nm laser irradiation; (c) steady-state FTIR spectra for duplex DNA ([AT7] = 3 mM) at pD 7.0 (red).

1658 cm^{-1}, and 1631 cm^{-1} [Fig. 6(a) and Table I]. The result is basically consistent with a previous report on the IR character of the TAT triplex.[31,47] The three bands are assigned to vibrational modes of thymine (1696 cm^{-1}, C2=O2 stretching mode; 1658 cm^{-1}, C4=O4 stretch; and 1631 cm^{-1}, ring vibrations for the third-strand Hoogsteen-bound thymines), among which the 1631 cm^{-1} peak is an indicator for the triplex structure. Distinct IR features are observed for its target duplex AT7 [Fig. 6(c) and Table I]. The C2=O2 and C4=O4 vibration modes for thymine are still observed at 1696 cm^{-1} and 1661 cm^{-1}. However, without the third-strand, the Hoogsteen-related 1631 cm^{-1} peak disappears and two new peaks at 1641 and 1623 cm^{-1} are observed. The 1641 cm^{-1} peak is due to the ring vibration of thymine involved in Watson–Crick base pairing. The 1623 cm^{-1} peak mainly corresponds to ND_2 scissoring modes of the A base, whose intensity is drastically reduced in the triplex due to hydrogen-bonding interactions with the third-strand thymine but recovers and becomes prominent in the duplex. The 1641 and 1623 cm^{-1} peaks are related to Watson-Crick base pairing in the duplex.[31,48]

With the knowledge of the typical IR features for the triplex distinct from the duplex, we then performed the FTIR experiments to examine the structural change for the TAT7 triplex following the one-electron oxidation by the $SO_4^{\bullet-}$ radical. It is first noticeable that in the control experiment performed for the TAT triplex alone irradiated by 355 nm laser, there are no changes observed in the IR spectra, meaning that the laser irradiation itself will not cause any reaction or structural change for the triplex. Interestingly, significant changes are observed in the IR spectra [Fig. 6(b) and Table I] recorded after 355 nm laser irradiation of the mixed solution of the TAT7 triplex with $Na_2S_2O_8$ ($SO_4^{\bullet-}$ precursor). With increasing irradiation time, the IR absorption peak at 1631 cm^{-1}, which is a feature of Hoogsteen hydrogen-bonding between the third strand and the homopurine strand of the target duplex, is found to diminish. It indicates that the Hoogsteen hydrogen bonding is disrupted after one-electron oxidation of the TAT triplex by $SO_4^{\bullet-}$. Concomitantly, two newly formed peaks at 1641 cm^{-1} and 1622 cm^{-1} are observed. As the irradiation time continue to increase to 8 min, the new peaks at 1622 cm^{-1} and 1641 cm^{-1} are more pronounced, as shown in Fig. 6(b) (green line). These bands do not change much after further 355 nm laser radiation longer than 8 min. Obviously, after 8 min of laser radiation the IR features are in full agreement with those of the duplex [Fig. 6(c)], confirming the conversion of the TAT7 triplex into a duplex as a result of one-electron oxidation. Considering that the TAT7 triplex is composed of continuous A bases and deprotonation of $A^{\bullet+}$ occurs with the N6-H proton Hoogsteen hydrogen-bonded with the third-strand, the disruption of continuous Hoogsteen hydrogen bonding is expected, which may result in the third strand dissociation, converting the triplex DNA into the duplex DNA. The IR and the laser flash photolysis results corroborate with each other. It shows here that the $A^{\bullet+}$ deprotonation following one-electron oxidation of the TAT triplex play key roles in the destruction of the triplex structure. Since the biological functions of the triplex such as gene expression and DNA mutagenesis highly rely on the structure,[18,25–27] the result here showing the triplex structure disruption by $A^{\bullet+}$ mediated oxidation and deprotonation has important implications.

TABLE I. Assignments for IR peaks (cm^{-1}) observed with triplex TAT7, duplex AT7, and one-electron oxidized TAT7 by $SO_4^{\bullet-}$.[a–d]

	TAT7	TAT7 + $SO_4^{\bullet-}$	AT7
C2=O2 (T)	1696	1696	1696
C4=O4 (T)	1658	1661	1661
Ring vibration (T: WC)		1641	1641
Ring vibration (T: Hoogs.)	1631		
ND_2 (A: WC)		1622	1623

[a]Spectra recorded in D_2O solutions.
[b]T, thymine; A, adenine; WC, base involved in Watson–Crick base pairing; Hoogs., base involved in Hoogsteen base pairing.
[c]TAT7: 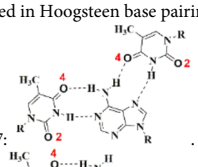 .
[d]AT7: 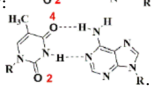 .

IV. CONCLUSIONS

In summary, we have directly observed the deprotonation process of $A^{\bullet+}$ in the TAT triplex after one-electron oxidation by time-resolved laser flash photolysis spectroscopy. The rate constants of TAT7 + $SO_4^{\bullet-}$ oxidation and $A^{\bullet+}$ deprotonation are 8.4×10^8 M^{-1} s^{-1} and 1.3×10^7 s^{-1} at room temperature, respectively. This rate constant for the deprotonation of $A^{\bullet+}$ in TAT7 is similar to that of duplex containing continuous A bases ($1.0–1.3 \times 10^7$ s^{-1}).[11] Furthermore, the deprotonation rate constants in H_2O and D_2O display KIE factors of 1.6 for dA and 1.8 for TAT7. Therefore, the proton of $A^{\bullet+}$ in TAT7 behaves as free proton to be directly released into the solvent.[36,37] Intriguingly, the FTIR spectra for the one-electron oxidized TAT triplex by $SO_4^{\bullet-}$ feature the disappearance of the Hoogsteen-related 1631 cm^{-1} peak and the concomitant emergence of the duplex IR peaks at 1641 cm^{-1} and 1622 cm^{-1}, suggesting that the $A^{\bullet+}$ mediated oxidation and deprotonation in the TAT triplex can disrupt the Hoogsteen hydrogen bond and then incur the structure instability, converting the triplex into the duplex DNA.

Overall, our results reveal that the presence of the third-strand has effects on the $A^{\bullet+}$ deprotonation behavior and the ensuing destruction of the triplex structure. For triplex TAT7, the proton surroundings differ from those in dA or in duplex, and the T in the third strand is paired with the A base in the target duplex by a Hoogsteen hydrogen bond. This structure results in greater water accessibility, given the high mobility of water in the inner hydrophilic part of the MM-groove.[21] Furthermore, the melting temperature of the third strand is lower than that of the duplex, which makes the amino protons of A base Hoogsteen-bound with the T base more likely to be released after one-electron oxidation. After the $A^{\bullet+}$ deprotonation with continuous A bases in triplex TAT7, the Hoogsteen hydrogen bonds are disrupted, causing the dissociation of the third strand. Thus, $A^{\bullet+}$ deprotonation may play a role in destabilization of the secondary structure of triplex DNA, and the triplex structure is less stable than the duplex. These results indicate that the third strand of

triplex may provide a unique structural platform with altered solvent accessibility and new hydrogen-bonding interaction, which renders triplex as a hotspot for DNA oxidative damage.

ACKNOWLEDGMENTS

This work was supported by the National Natural Science Foundation of China (Grant Nos. 21425313, 21727803, and 21933005).

REFERENCES

[1]T. Lindahl, Nature **365**, 700 (1993).
[2]A. Lapi, G. Pratviel, and B. Meunier, Met.-Based Drugs **8**, 47 (2001).
[3]G. V. Buxton, C. L. Greenstock, W. P. Helman, and A. B. Ross, J. Phys. Chem. Ref. Data **17**, 513 (1988).
[4]J. Choi, J. Park, A. Tanaka, M. J. Park, Y. J. Jang, M. Fujitsuka, S. K. Kim, and T. Majima, Angew. Chem., Int. Ed. **52**, 1134 (2013).
[5]A. Banyasz, T. M. Ketola, A. Munoz-Losa, S. Rishi, A. Adhikary, M. D. Sevilla, L. Martinez-Fernandez, R. Improta, and D. Markovitsi, J. Phys. Chem. Lett. **7**, 3949 (2016).
[6]Y. H. Wang, H. M. Zhao, Q. Zhou, X. J. Dai, K. H. Liu, D. Song, and H. M. Su, J. Phys. Chem. B **123**, 2853 (2019).
[7]S. Steenken, S. V. Jovanovic, M. Bietti, and K. Bernhard, J. Am. Chem. Soc. **122**, 2373 (2000).
[8]S. Steenken and S. V. Jovanovic, J. Am. Chem. Soc. **119**, 617 (1997).
[9]S. Steenken, Chem. Rev. **89**, 503 (1989).
[10]R. M. Scheek, S. Stob, T. Schleich, N. C. M. Alma, C. W. Hilbers, and R. Kaptein, J. Am. Chem. Soc. **103**, 5930 (1981).
[11]K. Kobayashi, J. Phys. Chem. B **114**, 5600 (2010).
[12]A. Kumar and M. D. Sevilla, Chem. Rev. **110**, 7002 (2010).
[13]D. M. Close, J. Phys. Chem. A **117**, 473 (2013).
[14]J. L. Jie, C. Wang, H. M. Zhao, D. Song, and H. M. Su, Chin. J. Chem. Phys. **30**, 664 (2017).
[15]G. Felsenfeld and A. Rich, Biochim. Biophys. Acta **26**, 457 (1957).
[16]J. Choi and T. Majima, Chem. Soc. Rev. **40**, 5893 (2011).
[17]A. S. Moffat, Science **252**, 1374 (1991).
[18]Y. Hu, A. Cecconello, A. Idili, F. Ricci, and I. Willner, Angew. Chem., Int. Ed. **56**, 15210 (2017).
[19]M. C. Linak, R. Tourdot, and K. D. Dorfman, J. Chem. Phys. **135**, 205102 (2011).
[20]B. J. Boehm, C. Whidborne, A. L. Button, T. L. Pukala, and D. M. Huang, Phys. Chem. Chem. Phys. **20**, 14013 (2018).
[21]G. C. Shields, C. A. Laughton, and M. Orozco, J. Am. Chem. Soc. **119**, 7463 (1997).
[22]Y. Rokhlenko, N. E. Geacintov, and V. Shafirovich, J. Am. Chem. Soc. **134**, 4955 (2012).
[23]V. Mohan, P. E. Smith, and B. M. Pettitt, J. Phys. Chem. **97**, 12984 (1993).
[24]C. Dohno, K. Nakatani, and I. Saito, J. Am. Chem. Soc. **124**, 14580 (2002).
[25]R. D. Wells, D. A. Collier, J. C. Hanvey, M. Shimizu, and F. Wohlrab, FASEB J. **2**, 2939 (1988).
[26]H. T. Lee, C. E. Carr, I. Khutsishvili, and L. A. Marky, J. Phys. Chem. B **121**, 9175 (2017).
[27]S. Walsh, A. H. El-Sagheer, and T. Brown, Chem. Sci. **9**, 7681 (2018).
[28]Q. G. Qi, C. F. Yang, Y. Xia, K. H. Liu, and H. M. Su, Acta Chim. Sin. **77**, 515 (2019).
[29]P. A. Beal and P. B. Dervan, Science **251**, 1360 (1991).
[30]A. M. Soto, J. Loo, and L. A. Marky, J. Am. Chem. Soc. **124**, 14355 (2002).
[31]C. Dagneaux, J. Liquier, and E. Taillandier, Biochemistry **34**, 14815 (1995).
[32]C. Dagneaux, H. Gousset, A. K. Shchyolkina, M. Ouali, R. Letellier, J. Liquier, V. L. Florentiev, and E. Taillandier, Nucleic Acids Res. **24**, 4506 (1996).
[33]A. M. Soto and L. A. Marky, Biochemistry **41**, 12475 (2002).
[34]J. L. Asensio, R. Carr, T. Brown, and A. N. Lane, J. Am. Chem. Soc. **121**, 11063 (1999).
[35]F. D. Lewis, Y. Wu, R. T. Hayes, and M. R. Wasielewski, Angew. Chem., Int. Ed. **41**, 3485 (2002).
[36]L. D. Wu, K. L. Liu, J. L. Jie, D. Song, and H. M. Su, J. Am. Chem. Soc. **137**, 259 (2015).
[37]K. Kobayashi, R. Yamagami, and S. Tagawa, J. Phys. Chem. B **112**, 10752 (2008).
[38]L. D. Wu, J. L. Jie, K. H. Liu, and H. M. Su, Acta Chim. Sin. **72**, 1182 (2014).
[39]W. J. Mcelroy, J. Phys. Chem. **94**, 2435 (1990).
[40]A. Adhikary, A. Kumar, D. Becker, and M. D. Sevilla, J. Phys. Chem. B **110**, 24171 (2006).
[41]A. Kumar and M. D. Sevilla, J. Phys. Chem. B **113**, 11359 (2009).
[42]A. A. Voityuk, J. Chem. Phys. **122**, 204904 (2005).
[43]M. J. Frisch, G. W. Trucks, H. B. Schlegel, G. E. Scuseria, M. A. Robb, J. R. Cheeseman, G. Scalmani, V. Barone, B. Mennucci, G. A. Petersson, H. Nakatsuji, M. Caricato, X. Li, H. P. Hratchian, A. F. Izmaylov, J. Bloino, G. Zheng, J. L. Sonnenberg, M. Hada, M. Ehara, K. Toyota, R. Fukuda, J. Hasegawa, M. Ishida, T. Nakajima, Y. Honda, O. Kitao, H. Nakai, T. Vreven, J. A. Montgomery, Jr., J. E. Peralta, F. Ogliaro, M. Bearpark, J. J. Heyd, E. Brothers, K. N. Kudin, V. N. Staroverov, T. Keith, R. Kobayashi, J. Normand, K. Raghavachari, A. Rendell, J. C. Burant, S. S. Iyengar, J. Tomasi, M. Cossi, N. Rega, J. M. Millam, M. Klene, J. E. Knox, J. B. Cross, V. Bakken, C. Adamo, J. Jaramillo, R. Gomperts, R. E. Stratmann, O. Yazyev, A. J. Austin, R. Cammi, C. Pomelli, J. W. Ochterski, R. L. Martin, K. Morokuma, V. G. Zakrzewski, G. A. Voth, P. Salvador, J. J. Dannenberg, S. Dapprich, A. D. Daniels, O. Farkas, J. B. Foresman, J. V. Ortiz, J. Cioslowski, and D. J. Fox, GAUSSIAN 09, Revision E.01, Gaussian, Inc., 2013.
[44]R. Lyng, A. Rodger, and B. Nordén, Biopolymers **32**, 1201 (1992).
[45]A. Adhikary, A. Kumar, D. Khanduri, and M. D. Sevilla, J. Am. Chem. Soc. **130**, 10282 (2008).
[46]A. Banyasz, T. Ketola, L. Martinez-Fernandez, R. Improta, and D. Markovitsi, Faraday Discuss. **207**, 181 (2018).
[47]J. Liquier, P. Coffinier, M. Firon, and E. Taillandier, J. Biomol. Struct. Dyn. **9**, 437 (1991).
[48]M. Tsuboi, Appl. Spectrosc. Rev. **3**, 45 (1970).